EUROPEAN ORGANISATION FOR NUCLEAR RESEARCH

CERN-PPE/91-52
15 March 1991

Precision Measurement of the Structure Function Ratios F_2^{He}/F_2^D, F_2^C/F_2^D and F_2^{Ca}/F_2^D

NEW MUON COLLABORATION (NMC)

Bielefeld University[1+], CERN[2], Freiburg University[3+], Max-Planck Institute Heidelberg[4+], Heidelberg University[5+], University of Mainz[6+], Mons University[7], Neuchâtel University[8], NIKHEF-K[9++], Oxford University[10], University of California, Santa Cruz[11], Paul Scherrer Institute[12], Torino University and INFN Torino[13], Uppsala University[14], Institute for Nuclear Studies, Warsaw[15], Warsaw University[16**], Wuppertal University[17+]*

P. Amaudruz[12a)], M. Arneodo[13], A. Arvidson[14], B. Badelek[16], G. Baum[1], J. Beaufays[9b)], I.G. Bird[4], M. Botje[12], C. Broggini[8c)], W. Brückner[4], A. Brüll[3], W.J. Burger[12d)], J. Ciborowski[16], R. van Dantzig[9], H. Döbbeling[4e)], J. Domingo[12f)], J. Drinkard[11], H. Engelien[3], M.I. Ferrero[13], L. Fluri[8], P. Grafstrom[14g)], D. von Harrach[4h)], M. van der Heijden[9], C. Heusch[11], Q. Ingram[12], K. Janson[14], M. de Jong[9], E.M. Kabuß[4h)], R. Kaiser[3], T.J. Ketel[9], F. Klein[6], B. Korzen[17], U. Krüner[17], S. Kullander[14], U. Landgraf[3], F. Lettenström[11], T. Lindqvist[14], G.K. Mallot[6], C. Mariotti[13], G. van Middelkoop[2,9], Y. Mizuno[4i)], J. Nassalski[15], D. Nowotny[4], N. Pavel[17j)], C. Peroni[13], H. Peschel[17k)], B. Povh[4,5], R. Rieger[6], K. Rith[4], K. Röhrich[6l)], E. Rondio[16], L. Ropelewski[16], A. Sandacz[15], C. Scholz[4], R. Schumacher[12m)], U. Sennhauser[12n)], F. Sever[1o)], T.-A. Shibata[5], M. Siebler[1], A. Simon[4], A. Staiano[13], G. Taylor[10p)], M. Treichel[4q)], J.L. Vuilleumier[8], T. Walcher[6], R. Windmolders[7], F. Zetsche[4]

(Submitted to Zeitschrift für Physik)

ABSTRACT

We present the structure function ratios F_2^{He}/F_2^D, F_2^C/F_2^D and F_2^{Ca}/F_2^D measured in deep inelastic muon-nucleus scattering at an incident muon momentum of 200 GeV. The kinematic range $0.0035 < x < 0.65$ and $0.5 < Q^2 < 90$ GeV^2 is covered. At low x the three ratios are significantly smaller than unity and the size of the depletion grows with decreasing x and increasing mass number A. At intermediate x the ratios show an enhancement of about 2% above unity for C/D and Ca/D, possibly less for He/D. There are indications of some Q^2 dependence in the Ca/D data. The integrals of the structure function differences $F_2^A - F_2^D$ are discussed.

For footnotes see next page

+ Supported by Bundersministerium für Forschung und Technologie.
++ Supported in part by FOM, Vrije Universiteit Amsterdam and NWO.
* Supported by CPBP.01.06.
** Supported by CPBP.01.09.

a) Now at TRIUMF, Vancouver, BC, Canada.
b) Now at Trasys, Brussels, Belgium.
c) Now at INFN, Laboratori Nazionali del Gran Sasso, 67010 Assergi, Italy.
d) Now at Université de Genève, 1211 Genève 4, Switzerland.
e) Now at GSI, 6100 Darmstadt, Germany.
f) Now at CEBAF, Newport News, VA, U.S.A.
g) Now at CERN, 1211 Geneva 23, Switzerland.
h) Now at University of Mainz, 6500 Mainz, Germany.
i) Now at Osaka University, Osaka, Japan.
j) Now at DESY, Hamburg, Germany.
k) Now at Gruner and Jahr AG & CoKG, Itzehoe, Germany.
l) Now at IKP2-KFA, Jülich, Germany,
m) Now at Carnegie Mellon University, Pittsburgh, U.S.A.
n) Now at EMPA, 8600 Dübendorf, Switzerland.
o) On leave from Jozef Stefan Institut, Ljubljana, Yugoslavia,
now at DPhN Saclay, 91191 Gif-sur-Yvette, France.
p) Now at University of Melbourne, Parkville, Victoria, Australia.
q) Now at Université de Neuchâtel, 2000 Neuchâtel, Switzerland.

The structure function F_2 of a bound nucleon differs from that of a free nucleon. This phenomenon, first observed by the European Muon Collaboration (EMC) [1], has stimulated a wide range of experimental [2–7] and theoretical activities [7,8].

The early CERN [1,3] and SLAC [2] experiments covered the region of intermediate to large x ($0.05 < x < 0.86$). The A dependence of the data was studied in detail at large x ($x > 0.3$) [2], where the deep inelastic scattering (DIS) process probes the valence quarks in the nucleon. Recent experiments have focussed on the small x region [5,6]. Attempts have also been made to investigate the phenomenon in neutrino and Drell-Yan experiments. While charged lepton scattering is sensitive to the sum of valence and sea quark distributions, experiments with neutrino beams are able to discriminate between quarks and anti-quarks. Neutrino experiments are however affected by large statistical and systematic uncertainties [7,9–11]. Drell-Yan experiments are sensitive to the anti-quark distribution and in one of them [12] effects similar to those seen in DIS have recently been observed.

At small x nuclear effects in structure functions are usually referred to as "shadowing". This has been described in terms of generalised vector meson dominance or of fusion mechanisms at the partonic level. At larger values of x, several classes of models have emerged. Conventional nuclear physics models take into account nuclear separation energies (leading to x–rescaling), nucleon-nucleon correlations and Fermi smearing; convolution models involve substructures other than nucleons inside the nucleus (e.g. pions, resonances, quark-clusters); Q^2 rescaling models invoke changes in the quark confinement size. In spite of the wealth of theoretical approaches proposed [7,8], no unique explanation of the EMC effect exists.

In deep inelastic charged lepton scattering from an unpolarised target the double differential cross section per nucleon can be written, in the one-photon exchange approximation, as

$$\frac{d^2\sigma_{1\gamma}}{dxdQ^2} = \frac{4\pi\alpha^2}{Q^4}\frac{F_2(x,Q^2)}{x}\left[1 - y - \frac{xyM}{2E} + \frac{y^2}{2}\left(\frac{1+4M^2x^2/Q^2}{1+R(x,Q^2)}\right)\right] \qquad (1)$$

Here $F_2(x,Q^2)$ is the structure function of the nucleon, $x = Q^2/2M\nu$ and $y = \nu/E$ are the scaling variables; E, ν and $-Q^2$ are the incident lepton energy, the energy transfer in the laboratory frame and the four momentum squared of the virtual photon, respectively. The mass M is the free proton mass and α is the electromagnetic coupling constant. The function $R(x,Q^2)$ is the ratio of the longitudinally to transversely polarized virtual photon absorption cross sections. Assuming R to be independent of the nuclear mass, the structure function ratios F_2^A/F_2^D are equal to the corresponding cross section ratios. This assumption is supported by recent data from SLAC [13] in the range $0.2 < x < 0.5$ and $1 < Q^2 < 5$ GeV^2.

In this paper we present results on the ratios of structure functions F_2^A/F_2^D for the isoscalar nuclei He, C and Ca. These three nuclei have comparable densities and binding energies per nucleon, while their mass numbers differ considerably. The structure function ratios for these targets were previously measured by SLAC-E139 [2] and EMC-NA2′ [5]. Our data however extend to much smaller values of x. Furthermore the statistical and systematic accuracy of the present results is superior to that of the EMC-NA28 results [6], which cover a similar range in the low x region up to $x \approx 0.1$.

The experiment was performed at the M2 muon beam line of the CERN SPS with a modified and upgraded version of the EMC spectrometer [5]. The mean incident muon momentum was 200 GeV with a 4 % spread (rms). Among the modifications to the EMC

set-up we mention those which are relevant to the data presented here. A more detailed description of the experimental apparatus can be found elsewhere [14].

Two independent trigger systems were used. Muon scattering angles larger than 12 mrad were covered by the standard trigger (T1), essentially the same as that of EMC. The small-angle trigger (T2) was sensitive to muons scattered between 5 and 15 mrad. Both triggers covered the region $x < 0.4$, the T2 events having smaller Q^2 and ν. Events at larger x were accepted by T1 only.

A complementary target set-up was used, allowing accurate measurements of cross section ratios on different target materials. Each target set consisted of a heavy target A (He, C or Ca) and a deuterium target D, simultaneously exposed to the beam, one behind the other along the beam direction. This set was frequently exchanged with a complementary one where target material A and deuterium were interchanged. Geometrical acceptance and efficiency corrections therefore cancel in the calculation of the ratios as do the beam fluxes. The frequent exchange of the two target sets (every 30 min, a total of a few hundred times) substantially eliminated the effects of possible time dependences of the apparatus acceptance and efficiency. The cross section ratio thus depends only on the number of events N and the number of nucleons T per unit area in the upstream (u) and downstream (d) targets:

$$\left(\frac{\sigma^A}{\sigma^D}\right)_{meas} = \sqrt{\frac{N_u^A \cdot N_d^A}{N_u^D \cdot N_d^D} \Big/ \frac{T_u^A \cdot T_d^A}{T_u^D \cdot T_d^D}} \quad . \tag{2}$$

The data discussed in this paper were collected with two different target configurations. In the first one, both complementary sets consisted of a 3 m long liquid helium and a 3 m long liquid deuterium target. The total target thicknesses were 37.8 g/cm^2 and 48.8 g/cm^2 for helium and deuterium, respectively. In the second configuration, two 1.1 m long liquid deuterium targets were interspersed with sets of C and Ca targets (see fig. 1), which consisted of several equally spaced slices distributed over a 1.1 m distance. The target thicknesses were in this case 18.7 g/cm^2 (C), 20.3 g/cm^2 (Ca) and 17.6 g/cm^2 (D). The calcium targets were kept in an argon atmosphere to avoid oxidation. The He, C and Ca targets were of natural isotopic composition. The deuterium targets contained 1.5% H atoms from a contamination of HD molecules.

The data were processed event by event using an upgraded version of the EMC programme chain [14], which performed pattern recognition and geometrical reconstruction of the incident and scattered muons and of the charged hadrons.

Cuts were applied in order to remove events from regions with rapidly changing acceptance (small scattering angle), poor spectrometer resolution (small ν) and high background from hadronic decays (low scattered muon energy). Also excluded was the kinematical region where the radiative corrections for the heavier nucleus in a given target combination exceeded a maximum value. This cut rejected events at large y and small x. The total number of events after applying the cuts is 0.65, 0.52 and 0.72 $\times 10^6$ for the He/D, C/D and Ca/D targets, respectively. The counts are equally divided between T1 and T2.

In order to correct the measured yields for higher order electromagnetic processes, the cross section ratio was calculated from eq. (2) after weighting each event with the factor $\eta = \sigma_{1\gamma}/\sigma_{meas}$. These radiative corrections were computed according to the prescription of Mo and Tsai [15]. The procedure corrects for the radiative tails of coherent elastic scattering

from nuclei and of quasi-elastic scattering from nucleons, as well as for the inelastic radiative tails.

In order to evaluate the coherent radiative tails the knowledge of the nuclear elastic form factors is required. Parametrisations of available data were used for deuterium [16] and for the heavy targets [17]. For the quasi-elastic tails the nucleon form factor parametrisation of Gari and Krümpelmann [18] was used. The reduction of the elastic nucleon cross section with respect to the free nucleon one (quasi-elastic suppression) was evaluated using the results of a calculation by Bernabeu [19] for deuterium, helium and carbon, whereas a Fermi gas approach [20] was applied for calcium. Finally, the evaluation of the inelastic tail requires the knowledge of both R and F_2 over a large range of x and Q^2. The function $R(x,Q^2)$ was taken from a fit [21] to the SLAC-E140 data. A fit [22] to the results of deep inelastic scattering experiments [6,21,23,24] and to low energy data in the resonance region [25] was used for F_2^D. The structure function F_2^A was obtained by multiplying F_2^D with an empirical fit to our cross section ratios together with the SLAC-E139 data [2] for $x > 0.4$. Since the measured ratio is needed as an input, an iterative procedure is required. The radiative correction factors η for the individual targets range from the cutoff value of 0.6 at small x to 1.1 at large x. The resulting mean corrections to the ratios are 7 %, 17 % and 24 % at the lowest x for He/D, C/D and Ca/D, respectively. They decrease rapidly with increasing x and are less than 1 % for $x > 0.025$.

Figure 1 shows the distribution of reconstructed vertices along the beam direction in the measurement of Ca/D and C/D. The attribution of events to the wrong target was estimated from an extrapolation of the tails of these distributions. The largest correction to the ratio from this source was 0.4 %, at the smallest x value.

The target thicknesses were corrected to account for scattering in the air and argon between the carbon and calcium slices, and in the mylar windows of the liquid targets. A correction was also applied to take into account the slight non-isoscalarity of the targets. Finally, the effects of the limited spectrometer resolution in x and Q^2 (smearing effects) on the ratio were estimated by a Monte Carlo simulation of the experiment. The total effect of all the above corrections on the ratio was less than 1 %.

For each of the three target pairs the data from both triggers were analysed separately and the results were found to agree in the region of overlap. Figure 2 and table 1 show the x dependence of the structure function ratios, averaged over Q^2. The Q^2 range, the mean Q^2 and y for each x bin are also given in table 1. The data cover the range $0.0035 < x < 0.65$ and $0.5 < Q^2 < 90$ GeV^2. The inner error bars in fig. 2 show the statistical errors, the outer error bars include the systematic errors added in quadrature. Both the statistical and the systematic errors at small x are typically 1 %. The quadratic sum of the individual contributions to the systematic errors is dominated at small x by the uncertainties in the radiative corrections. An additional systematic error of 0.5 % is included over the whole x range as an estimate of the uncertainty of the complementary target method used to extract the ratios. The normalisation uncertainty on the ratios is not included in the errors shown in fig. 2 nor in table 1. It is essentially due to the errors on the target thicknesses and amounts to 0.4 %. At small x, the results for the structure function ratios are sensitive to the assumption $\Delta R = R^A - R^D = 0$. For instance, if $\Delta R = \pm 0.05$, then the ratios will change by up to ± 1 % at small x.

All three structure function ratios show a characteristic x dependence. There is a depletion below unity at small x, which increases with decreasing x. The size of the depletion is about 7 %, 12 % and 22 % in the lowest x bin for He/D, C/D and Ca/D, respectively. The results thus show a clear difference in shadowing between nuclei of similar binding

energies and nuclear densities but of considerably different mass numbers. The data show a clear enhancement at intermediate x, of about 2 % for C/D and Ca/D, and possibly less for He/D.

In fig. 3 we compare our data to those of previous measurements. The NMC results for He/D are the first to cover the low x region. In the same region the C/D and Ca/D ratios were previously measured by the EMC [6], but the present data are more precise. In the intermediate x region, where the data were so far inconclusive, an enhancement of the C/D and Ca/D ratios above unity is now clearly visible. At large x, the NMC results are consistent with the well known EMC effect shape [2–5].

In the measured Q^2 range there is little indication of a Q^2 dependence of the ratios. Figure 4 shows the structure function ratios versus Q^2 at fixed values of x. The logarithmic slopes b obtained from fits of the type $F_2^A/F_2^D = a + b \ln Q^2$ in each bin separately are shown in fig. 5 for x up to 0.45. For He/D and C/D no significant Q^2 dependence is observed. In the case of Ca/D we find negative slopes over a large fraction of the x range. Only in a few bins, however, are they different from zero in a statistically significant way.

From the structure function ratio and the absolute structure function F_2^D, the difference $F_2^A - F_2^D$ can be evaluated as $(F_2^A/F_2^D - 1)F_2^D$ and thus the integral $\int (F_2^A - F_2^D)dx$ can be computed. In the framework of the quark-parton model this integral, evaluated over the full x range, represents the difference of the momentum fraction carried by charged partons in bound nucleons relative to that for deuterium. To account for target mass effects the integration must be carried out over the Nachtmann scaling variable ξ [26,27]. For this purpose the integrand is multiplied by a function $K_2(x, Q^2)$ close to unity[1]. Furthermore, the integrands must include the correction $f_M = (AM/M_A - 2M/M_D)$ due to the mass defect of bound nucleons; M_A, M_D are the masses of nucleus A and of deuterium, respectively.

Table 2 shows the values of the integrals up to $x = 0.25$. They were derived taking the same parametrisation[2] for the structure function F_2^D that was used to calculate radiative corrections, evaluated at $Q^2 = 5$ GeV^2. No Q^2 dependence was assumed for the ratios. The systematic errors include the contributions of the systematic errors on the measured points and their normalisation uncertainty, as well as the uncertainty on F_2^D [22]. The same integrals can be computed after evaluating the NMC data at $Q^2 = 5$ GeV^2 with the above mentioned fits to the points of fig. 4. The amount by which the results vary if this procedure is adopted is at most of the size of the systematic errors. Furthermore the statistical errors then become about twice as large. The assumption that R^A differs from R^D by 0.05 affects the results of table 2 by less than 0.2×10^{-3}.

The data of the SLAC experiment E139 [2] were used to extend the integration for x larger than 0.25. No Q^2 dependence was assumed for these data either and their systematic errors were taken from [28]. The results of the integrals thus found are also shown in table 2. In the range covered by the NMC and SLAC results the integrals appear to be negative and to decrease with the nuclear mass number A. Note that the available data do not allow the evaluation of the integrals over the full x range.

In summary, we have measured the x and Q^2 dependence of the EMC effect at small x for helium, carbon and calcium. The shadowing signal at small x becomes stronger at larger A and shows no significant dependence on Q^2. The structure function ratios show an enhancement above unity at intermediate x, particularly significant for F_2^C/F_2^D

[1] Using the nomenclature of ref. [26] this function reads:
$K_2(x,Q^2) = \sqrt{1+\frac{4M^2x^2}{Q^2}}\left(\frac{2}{1+\sqrt{1+4M^2x^2/Q^2}}\right)\left(1-\frac{(M\xi)^4}{Q^4}\right)(1+3\eta_2)$.

[2] With this parametrisation $\int_0^1 F_2^D(x)K_2(x)dx = 0.148$, at $Q^2 = 5$ GeV^2.

and F_2^{Ca}/F_2^D. There are indications that the integrals $\int (F_2^A - F_2^D)dx$, evaluated over the range covered by this experiment and by SLAC-E139 [2], are negative and decrease with increasing mass number.

References

[1] EMC-NA2, J.J. Aubert *et al.*, Phys. Lett. **123B** (1983) 275

[2] SLAC-E139, R.G.Arnold *et al.*, Phys. Rev. Lett. **52** (1984) 727;
R.G.Arnold, SLAC-PUB-3257 (1983)

[3] BCDMS, G. Bari *et al.*, Phys. Lett. **163B** (1985) 282

[4] BCDMS, A.C. Benvenuti *et al.*, Phys. Lett. **B 189** (1987) 483

[5] EMC-NA2′, J. Ashman *et al.*, Phys. Lett. **B 202** (1988) 603

[6] EMC-NA28, M. Arneodo *et al.*, Nucl. Phys. **B333** (1990) 1

[7] For a review of the experimental and theoretical situation see e. g. :
T. Sloan, G. Smadja and R. Voss, Phys. Rep. **162** (1988) 45

[8] For a review of the theoretical models see e. g. :
L. Frankfurt and M. Strikman, Phys. Rep. **160** (1988) 235;
R.J.M. Covolan and E. Predazzi, in "Problems of Fundamental Modern Physics", Editors R. Cherubini, P. Dalpiaz and B. Minetti, World Scientific, Singapore (1991) p. 85

[9] FNAL-E745, T. Kitagaki *et al.*, Phys. Lett. **B 214** (1988) 281

[10] WA59, J. Guy *et al.*, Phys. Lett. **B 229** (1989) 421

[11] WA59, P.P. Allport *et al.*, Phys. Lett. **B 232** (1989) 417

[12] FNAL-E772, D.M. Alde *et al.*, Phys. Rev. Lett. **64** (1990) 2479

[13] SLAC-E140, S. Dasu *et al.*, Phys. Rev. Lett. **60** (1988) 2591

[14] NMC, D. Allasia *et al.*, Phys. Lett. **B 249** (1990) 366 and references cited therein

[15] L.W. Mo and Y.S. Tsai, Rev. Mod. Phys. **41** (1969) 205;
Y. S. Tsai, SLAC-PUB-848 (1971)

[16] A. Švarc and M.P. Locher, Fizika **22** (1990) 549;
M.P. Locher and A. Švarc, Z. Phys. **A 338** (1991) 89

[17] I. Sick, Phys. Lett. **116B** (1982) 212;
I. Sick, Nucl. Phys. **A218** (1974) 509;
I. Sick *et al.*, Phys. Lett. **88B** (1979) 245;
H. De Vries *et al.*, Atomic Data and Nuclear Data Tables, **36** (1987) 495

[18] M. Gari and W. Krümpelmann, Z. Phys. **A 322** (1985) 689

[19] J. Bernabeu, Nucl. Phys. **B49** (1972) 186

[20] E.J. Moniz, Phys. Rev. **184** (1969) 1154

[21] L.W. Whitlow, SLAC-Report 357 (1990);
L.W. Whitlow *et al.*, Phys. Lett. **B 250** (1990) 193

[22] NMC, P. Amaudruz *et al.*, CERN-PPE/91-05 (1991)

[23] CHIO, B.A. Gordon *et al.*, Phys. Rev. **D 20** (1979) 2645

[24] BCDMS, A.C. Benvenuti *et al.*, Phys. Lett. **B 237** (1990) 599;
BCDMS, A.C. Benvenuti *et al.*, Phys. Lett. **B 237** (1990) 592

[25] M.D. Mestayer, Ph.D. thesis, Stanford University, SLAC-Report 214 (1978)

[26] O. Nachtmann, Nucl. Phys. **B78** (1974) 455

[27] H. Georgi and H.D. Politzer, Phys. Rev. **D 14** (1976) 1829

[28] J. Gomez, Ph.D. thesis, The American University, Washington D.C. (1987)

x	$\langle Q^2 \rangle$[GeV^2]	Q^2 range [GeV^2]	$\langle y \rangle$	F_2^{He}/F_2^D	stat.	syst.
0.0035	0.77	0.5 – 1.2	0.65	0.931	0.026	0.022
0.0055	1.3	0.7 – 2.2	0.65	0.944	0.011	0.018
0.0085	1.8	0.9 – 3.1	0.59	0.966	0.011	0.014
0.0125	2.4	1.1 – 4.4	0.53	0.954	0.009	0.011
0.0175	3.0	1.1 – 6.2	0.47	0.982	0.009	0.009
0.025	3.8	1.1 – 9.2	0.42	0.986	0.008	0.008
0.035	4.7	1.1 – 12	0.37	0.991	0.009	0.007
0.045	5.6	1.3 – 15	0.34	1.003	0.010	0.007
0.055	6.3	1.5 – 18	0.31	1.005	0.011	0.007
0.070	7.3	1.8 – 24	0.29	0.990	0.009	0.006
0.090	8.7	2.4 – 25	0.26	1.021	0.010	0.006
0.125	11	2.9 – 43	0.24	0.998	0.008	0.006
0.175	14	4.7 – 46	0.22	1.018	0.011	0.005
0.25	19	5.9 – 62	0.21	0.995	0.011	0.005
0.35	24	13 – 86	0.19	0.985	0.019	0.005
0.45	31	17 – 87	0.19	0.923	0.029	0.005
0.55	38	21 – 90	0.19	0.949	0.051	0.005
0.65	44	27 – 64	0.18	1.049	0.085	0.005

x	$\langle Q^2 \rangle$[GeV^2]	Q^2 range [GeV^2]	$\langle y \rangle$	F_2^C/F_2^D	stat.	syst.
0.0035	0.74	0.5 – 0.9	0.62	0.879	0.018	0.016
0.0055	1.2	0.7 – 1.9	0.57	0.906	0.011	0.010
0.0085	1.7	0.9 – 2.7	0.54	0.909	0.011	0.008
0.0125	2.3	0.9 – 4.3	0.51	0.915	0.009	0.007
0.0175	3.0	1.1 – 6.2	0.47	0.944	0.010	0.006
0.025	3.8	1.1 – 9.2	0.42	0.949	0.008	0.006
0.035	4.9	1.3 – 12	0.38	0.976	0.009	0.005
0.045	6.0	1.7 – 15	0.37	0.969	0.010	0.005
0.055	7.2	2.0 – 18	0.36	0.996	0.012	0.005
0.070	8.8	2.4 – 24	0.34	1.018	0.010	0.005
0.090	11	3.3 – 26	0.33	1.031	0.012	0.005
0.125	14	4.0 – 35	0.31	1.019	0.009	0.005
0.175	17	5.9 – 46	0.27	1.017	0.012	0.005
0.25	21	8.5 – 60	0.23	1.001	0.012	0.005
0.35	26	13 – 80	0.21	0.966	0.018	0.005
0.45	31	17 – 84	0.19	1.011	0.030	0.006
0.55	37	21 – 88	0.19	0.960	0.046	0.006
0.65	42	27 – 86	0.17	0.843	0.062	0.007

x	$\langle Q^2 \rangle$[GeV^2]	Q^2 range [GeV^2]	$\langle y \rangle$	F_2^{Ca}/F_2^D	stat.	syst.
0.0035	0.60	0.5 – 0.8	0.47	0.780	0.021	0.019
0.0055	0.94	0.7 – 1.6	0.46	0.782	0.009	0.013
0.0085	1.4	0.7 – 2.6	0.43	0.831	0.009	0.010
0.0125	1.9	0.8 – 3.7	0.41	0.859	0.007	0.008
0.0175	2.5	0.9 – 5.2	0.40	0.899	0.008	0.007
0.025	3.4	0.9 – 9.2	0.38	0.938	0.006	0.006
0.035	4.7	1.3 – 12	0.36	0.949	0.007	0.005
0.045	5.7	1.6 – 15	0.35	0.978	0.009	0.005
0.055	6.8	2.0 – 18	0.34	0.966	0.010	0.005
0.070	8.1	2.4 – 24	0.32	0.988	0.008	0.005
0.090	9.7	3.3 – 25	0.30	1.020	0.010	0.005
0.125	12	4.0 – 34	0.26	1.022	0.008	0.005
0.175	14	5.9 – 45	0.23	1.034	0.010	0.005
0.25	19	8.4 – 61	0.21	0.983	0.010	0.005
0.35	24	13 – 79	0.19	0.984	0.017	0.006
0.45	30	17 – 83	0.19	0.929	0.027	0.006
0.55	35	21 – 85	0.18	0.869	0.042	0.006
0.65	41	27 – 85	0.17	0.917	0.067	0.007

Table 1: The structure function ratios F_2^A/F_2^D averaged over Q^2. The normalisation uncertainty of 0.4 % is not included in the systematic errors.

	x range	$\int \left(\frac{F_2^A}{F_2^D}(x) - 1 + f_M\right) F_2^D(x) \cdot K_2(x) dx$	stat.	syst.
He/D	$0.0035 - 0.25$	0.6×10^{-3}	0.3×10^{-3}	0.6×10^{-3}
	$0.0035 - 0.86$	-0.8×10^{-3}	0.4×10^{-3}	2.2×10^{-3}
C/D	$0.0035 - 0.25$	0.7×10^{-3}	0.3×10^{-3}	0.5×10^{-3}
	$0.0035 - 0.78$	-1.6×10^{-3}	0.7×10^{-3}	1.4×10^{-3}
Ca/D	$0.0035 - 0.25$	0.0×10^{-3}	0.3×10^{-3}	0.6×10^{-3}
	$0.0035 - 0.78$	-3.5×10^{-3}	0.6×10^{-3}	1.4×10^{-3}

Table 2: Integrals of the structure function differences $F_2^A - F_2^D$. For an explanation of the symbols and of the integration ranges see text.

Figure 1: Distribution of reconstructed vertices along the beam direction in the measurement of Ca/D and C/D. The cylindrical liquid deuterium targets and the solid targets, which consisted of four calcium and five carbon slices, are clearly resolved. The small peak in the centre results from events scattered off a proportional chamber (P0B).

Figure 2: Structure function ratios as functions of x, averaged over Q^2. The inner error bars indicate statistical errors only, the outer ones include the systematic errors added in quadrature. The 0.4% normalisation uncertainty is not included.

Figure 3: Comparison of the NMC structure function ratios with corresponding results from other experiments: SLAC-E139 [2], EMC-NA2′ [5] and EMC-NA28 [6]. Also shown are the F_2^N/F_2^D data from BCDMS [3]. The error bars show the statistical and systematic errors added in quadrature.

Figure 4: The structure function ratios as a function of Q^2 in each x bin. The errors shown are statistical only.

Figure 5: The slopes b from a linear fit in $\ln Q^2$ for each x bin separately, up to $x = 0.45$. The errors shown are statistical only.

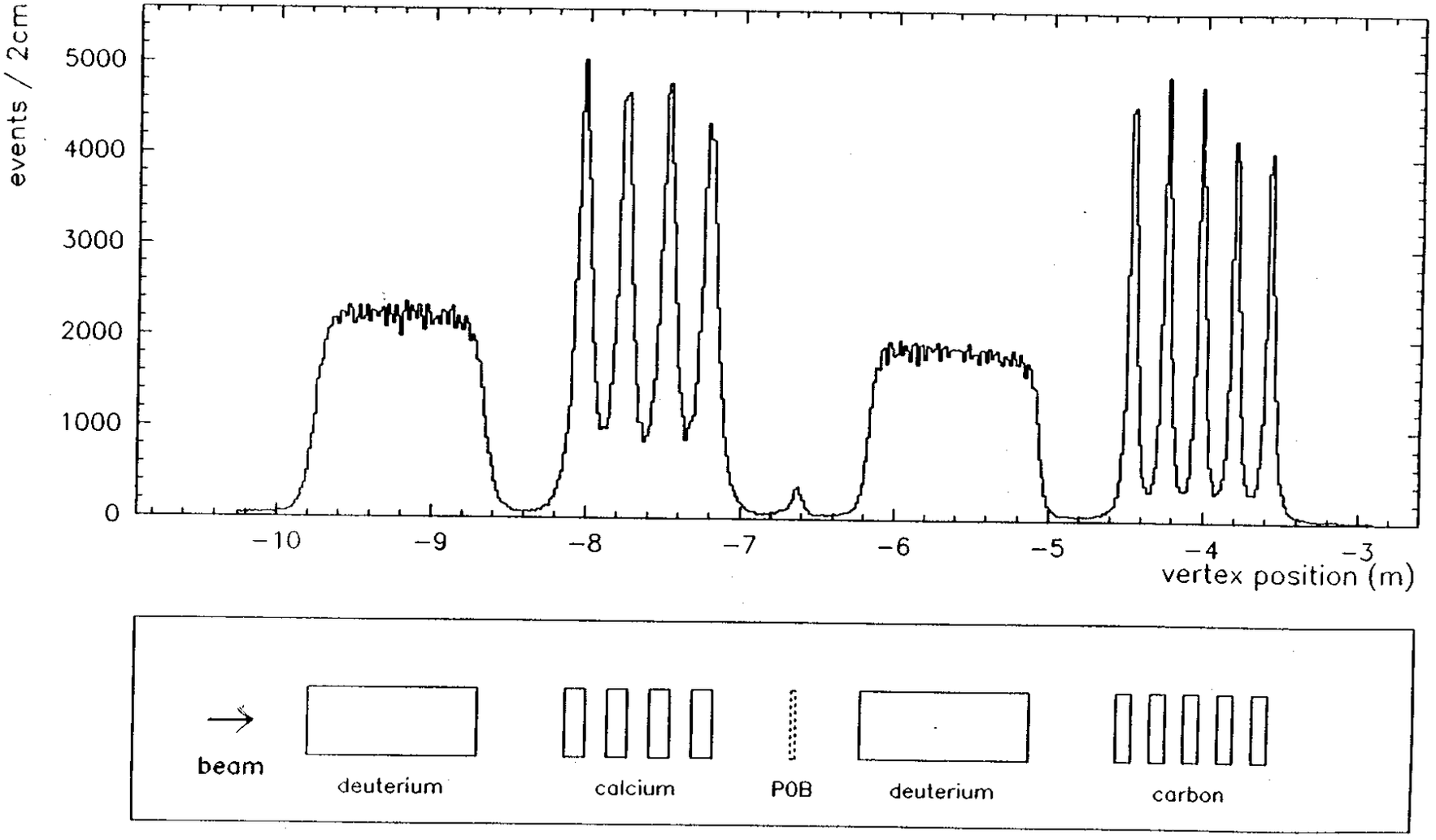
events / 2cm
5000
4000
3000
2000
1000
0
−10
−9
−8
−7
−6
−5
−4
−3
vertex position (m)
beam
deuterium
calcium
POB
deuterium
carbon

Fig. 1

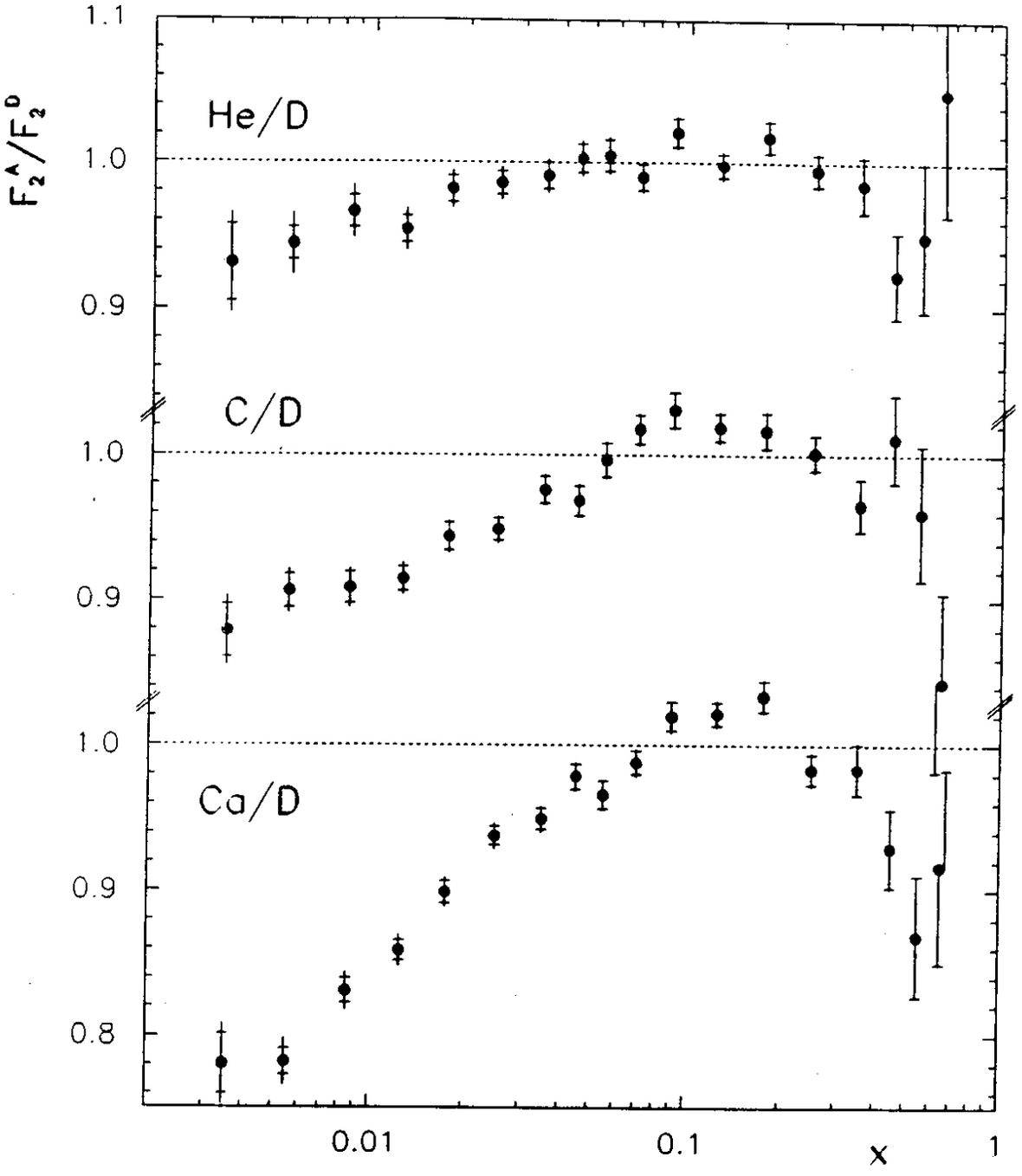

Fig.2

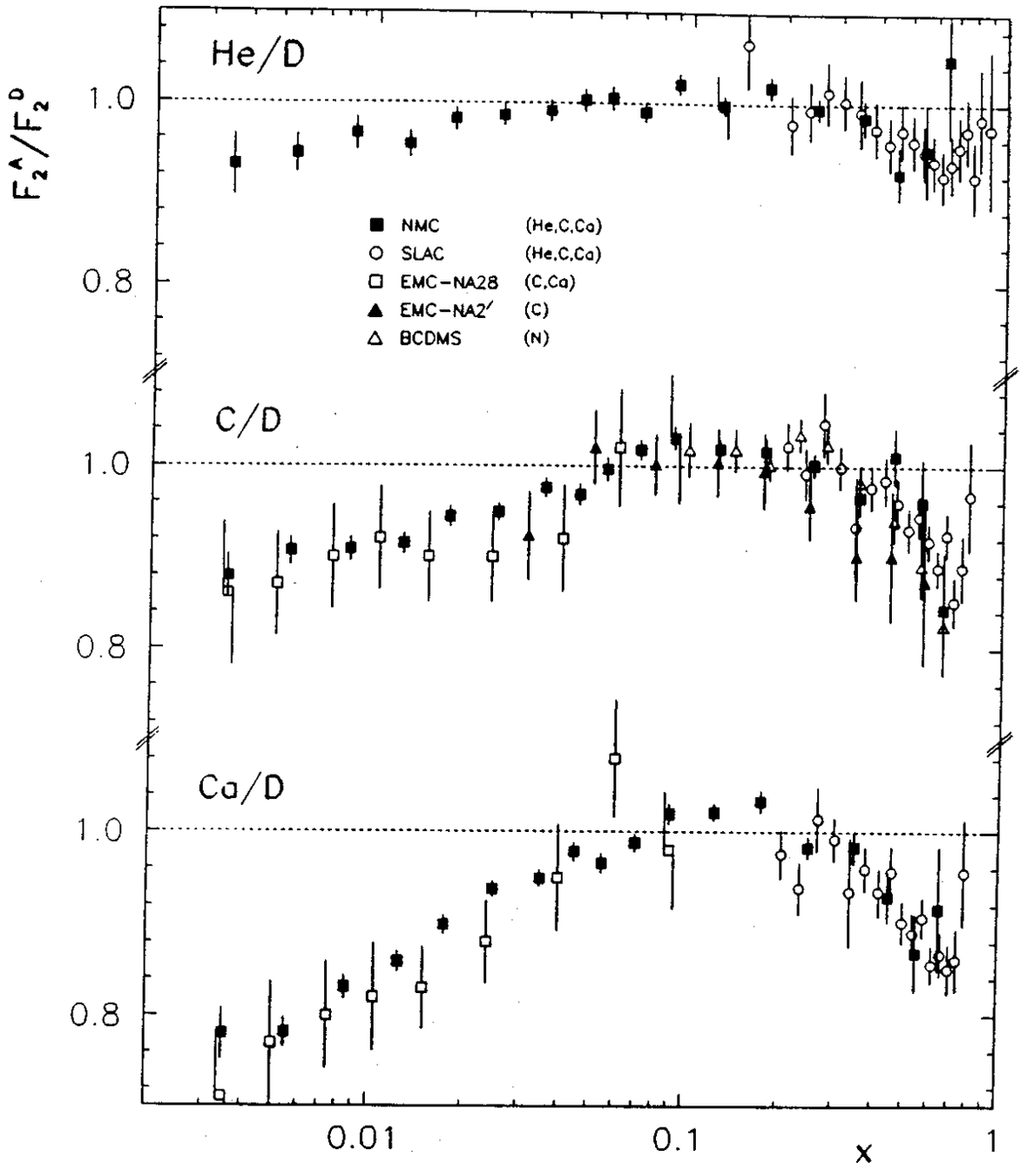
He/D
C/D
Ca/D
F_2^A/F_2^D
1.0
0.8
NMC (He,C,Ca)
SLAC (He,C,Ca)
EMC-NA28 (C,Ca)
EMC-NA2' (C)
BCDMS (N)
0.01
0.1
1
x

Fig. 3

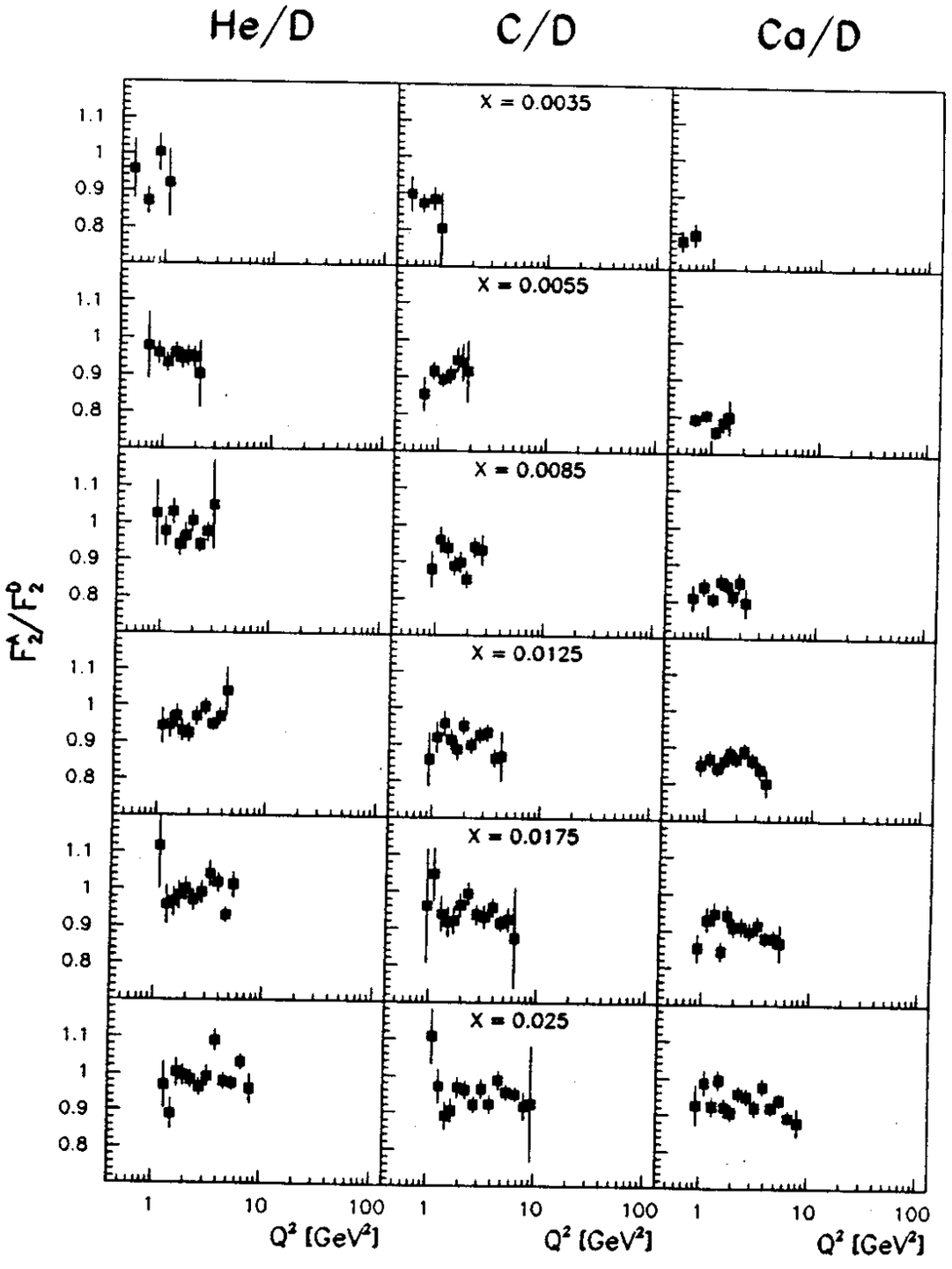
He/D
C/D
Ca/D
X = 0.0035
X = 0.0055
X = 0.0085
X = 0.0125
X = 0.0175
X = 0.025
F_2^A/F_2^D
1.1
1
0.9
0.8
1
10
100
Q^2 [GeV^2]

Fig. 4a

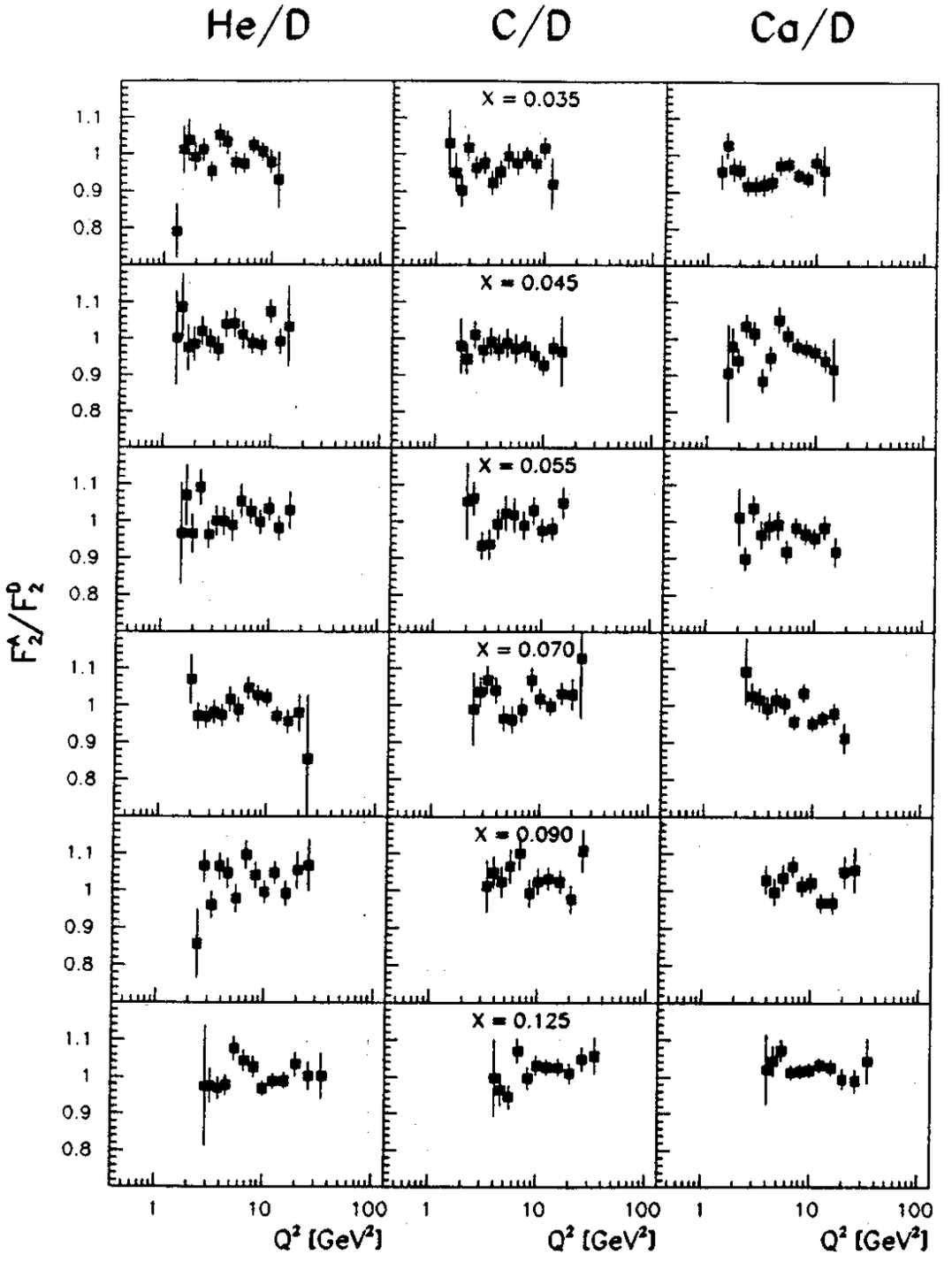
He/D
C/D
Ca/D
X = 0.035
X = 0.045
X = 0.055
X = 0.070
X = 0.090
X = 0.125
F_2^A/F_2^D
1.1
1
0.9
0.8
1
10
100
Q^2 [GeV^2]

Fig. 4b

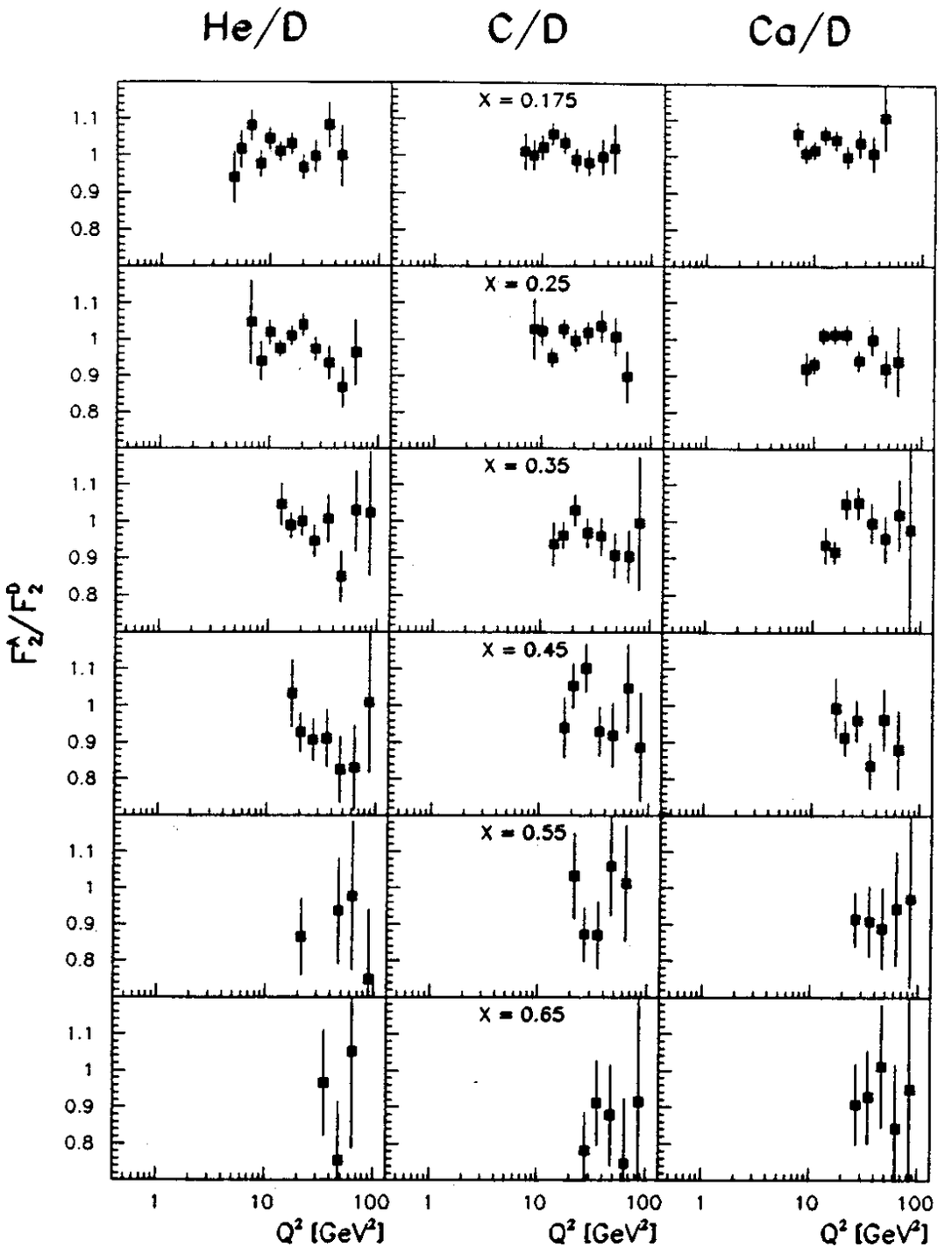
He/D
C/D
Ca/D
X = 0.175
X = 0.25
X = 0.35
X = 0.45
X = 0.55
X = 0.65
F_2^A/F_2^D
Q^2 [GeV^2]
1.1
1
0.9
0.8
1
10
100

Fig. 4c

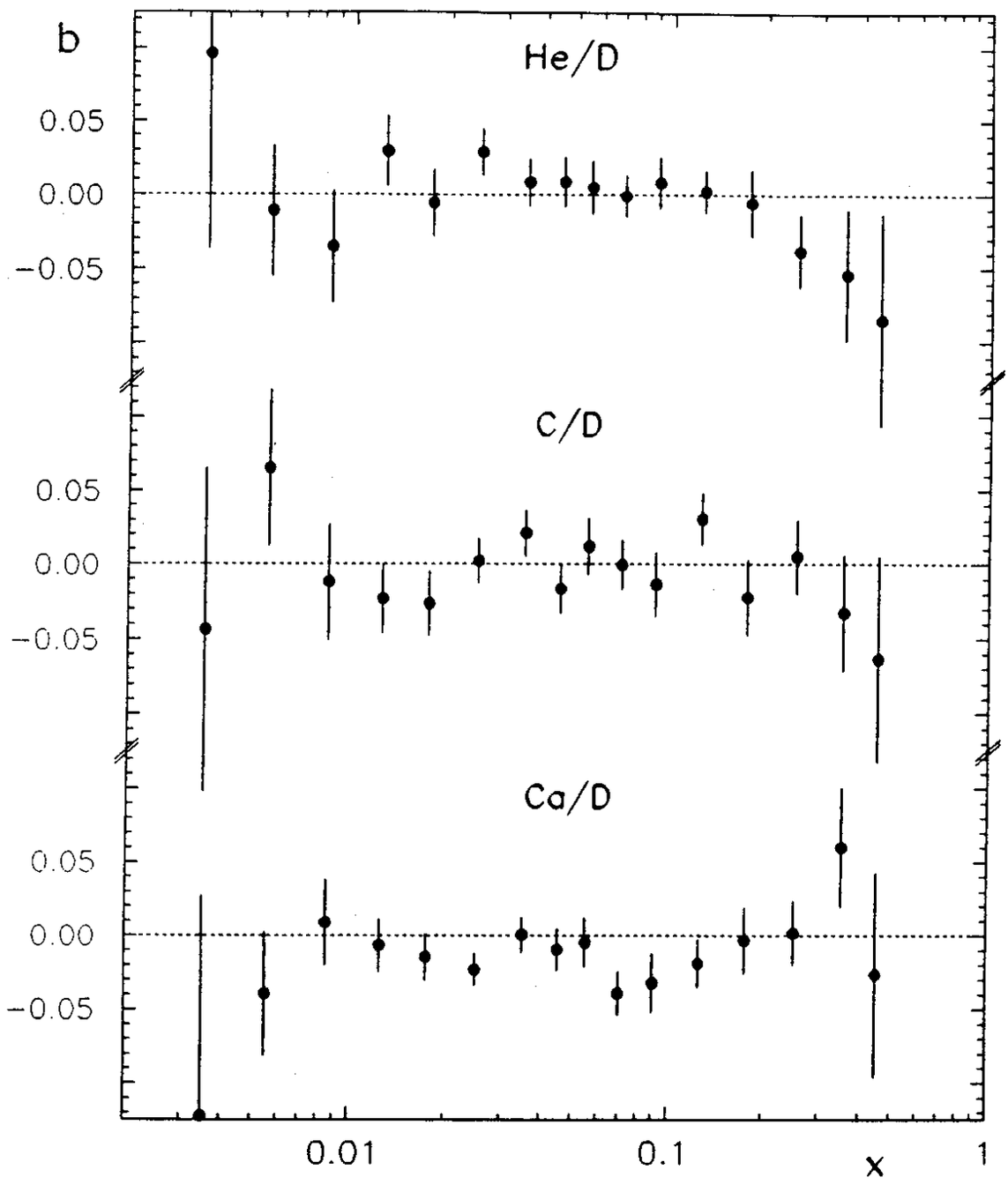

Fig. 5

Imprimé au CERN. Prix : 0.60 Fr.